Biomass Conversion and Biorefinery (2024) 14:17301–17311
https://doi.org/10.1007/s13399-023-03783-z

ORIGINAL ARTICLE

Visible light photocatalytic degradation of organic pollutants in industrial wastewater by engineered TiO_2 nanoparticles

Aakanksha Rajput[1] · Md Azizur Rahman[2] · Md Hafizur Rahman[3] · Arindam Kuila[1]

Received: 11 November 2022 / Revised: 2 January 2023 / Accepted: 9 January 2023 / Published online: 16 January 2023

Abstract

The present study acknowledges a simple and effective sol–gel: doping method was used for band-gap engineering of titanium dioxide (TiO_2) nanoparticles at lowest temperature (40 ℃) to produce doped TiO_2 with dopants like N (nitrogen), C (carbon), Ag (silver), and Fe (iron) of different concentrations that decreased band-gap energies (i.e., > 3.2 eV) from UV range to visible range. Structural and functional properties were modulated by controlling the composition of dopants and precursors for better adsorption property and high specific surface area. Tauc-plot with UV–Vis spectrum: N (2.1 eV) > C (2.8 eV) > Ag (2.9 eV) > Fe (3.0 eV) suggested reduced band-gap energies (i.e., ≥ 3.0 eV). The photocatalytic effect was verified with the degradation of methylene blue (MB) and acid pink dye under visible light irradiation. Observation suggested that nitrogen-doped TiO_2 (N-TiO_2) with 2%wt. concentration has shown a higher degradation rate of 74% with respect to methylene blue in 60 min. A total of 98.4% degradation of acid pink dye (widely used in textile industry) was performed in 60 min by Fe2 (iron-doped TiO_2 with 2% wt). The doped-TiO_2 nanoparticles were also verified for their antimicrobial activity toward pathogenic strain. XRD (X-ray diffraction) revealed that the doped TiO_2 nanoparticles had attained anatase structure at a lower temperature without calcination process as compared to the reported literature.

Keywords Engineered TiO_2 · Dopants · Band-gap energy · Photocatalytic effect · Waste-water treatment

1 Introduction

Titanium dioxide (TiO_2) nanomaterials are incredible photocatalysts among all available metal oxides that gain the great interest of researchers on account of their effective and exceptional properties such as great photo-catalytic activity; negligible toxicity; corrosion resistance; inexpensive, easy to modify, thermodynamic stability; and a high compatible factor. Additionally, engineered TiO_2 has achieved wide applicability in different domains from bioscience to space science such as for the synthesis of inverted heterojunction solar cell devices, elimination of environmental pollutants, dye degradation, hydrogen generation, pesticides, popular photoanode material in DSSCs (dye-sensitized solar cells) and heavy metal adsorption [1–3]. TiO_2 has three crystal forms, namely, anatase, rutile, and brookite based on their lattice arrangement. According to structural aspect, anatase is zigzag structure where every octahedron shares four edges with another four octahedrons; brookite has a crystalline structure where every octahedron shares three edges with tunnels along the c-axis and in rutile phase, formation of linear chains along the direction [001] is performed by sharing of two octahedrons, and the TiO6 chains are linked to each other through corned shared bondings. Among all three forms, anatase and brookite are considered metastable that transformed to rutile after heating, and rutile is reported the stable form [4]. The defined lattice arrangement of anatase makes it highly photoactive and commonly utilized in photocatalysis among these three types. Based on optical activation property, all three forms of TiO_2 have

✉ Md Azizur Rahman
azizur.iitd@gmail.com

✉ Arindam Kuila
arindammcb@gmail.com

[1] Department of Bioscience and Biotechnology, Banasthali Vidyapith, Tonk, Rajasthan 304022, India

[2] Department of Biotechnology Engineering and Food Technology, University Institute of Engineering, Chandigarh University, H-05, Ludhiana- Chandigarh State Hwy, Sahibzada Ajit Singh Nagar, Punjab 140413, India

[3] Centre for Environmental Studies, The Energy and Resources Institute, IHC Complex, Lodhi Road, New Delhi 110003, India

different band gaps, and stable phases likely anatase (band gap = 3.2 eV) and brookite (band gap = 2.96 eV) have metastable phase, and rutile (band-gap = 3.0 eV) has most stable phase [5, 6]. Although all phases of TiO_2 (anatase, brookite, and rutile) have larger band-gap energies suitable for an optical absorption edge in the UV range (ultraviolet range); however, the absorption is not activated in the VIS range (visible light range). This wide band-gap energy (3.2 eV) of TiO_2 nanoparticles restricts its uses and application. In the same context, to overcome this drawback, engineering of TiO_2 nanomaterials performed via doping has been realized as an effective approach since electron trapping magnifies the electron–hole dissociation, upgrades the photocatalyst surface properties, and amplifies surface electron excitation by plasmon resonances elevated by visible light [7, 8]. Especially for the modification of inorganic semiconductors, metal and nonmetal doping is a very appropriate and efficient method. It supports the synthesis of visible light-responsive TiO_2 photo-catalysts, decreasing its wide band gap [9]. The remarkable response has been reported by some non-metal anions including B, C, I, N, S, and some metal cations such as Cr, Fe**,** Ag**,** V for the extension of photo-response of semiconductors toward the visible light range [10, 11]. According to Habibi and Jamshidi [12], C-doped TiO_2 nanoparticles have registered upgraded photocatalytic performance in visible light, prepared by sol–gel process. They reported that 51.18% methylene blue degradation was traced in the aqueous phase of degradation. Regarding Ag dopant, Abbad et al. [7] has informed that 10%-weight Ag-doped TiO_2 nanoparticles can perform complete degradation of methylene blue. Sood et al. [13] explained that, at 0.05 mol% Fe^{3+} molar concentrations, Fe-doped TiO_2 nanoparticles were able to degrade 92% of para-nitrophenol in 5 h by following hydrothermal method. By addition of nitrogen precursor for synthesis of N-doped TiO_2, nanoparticles gave excellent outcomes for photocatalytic activity of catalyst under visible light. N:TiO_2 (1.5 at.%) ratio concluded a reduction in band gap from 3.2 to a minimum of 2.79 eV [14]. Though economic growth of the country majorly dependent on the textile manufacturing but simultaneously high levels of virulent and undesirable dyes released from textile and leading imbalance in the integrity of the ecosystem that causing environmental pollution. Among the verities of dyes, acid dyes are immensely used in industry as they are considered water-soluble anionic dyes and broadly applied to modified acrylics, wool, nylon, and silk. Photocatalysis is a considerable tool for effective degradation of dye from pollutant water [15]. In remediation aspect, TiO_2 is assumed the most commonly applied and efficient photocatalyst with promising application in dye degradation from aqueous solution as textile wastewater (major challenge of the municipal world) became an alarming issue toward people health and environment [16]. Various types of nanoparticles including ZnO, Ag, TiO_2 and many have been reported noticeable antimicrobial activity with respect to diverse microbial sources such as *Brucella abortus*, *Candida albicans*, and *Salmonella typhimurium* [17]. TiO_2 nanoparticles have also great potential for inhibition of pathogenic microorganisms gram positive (*Bacillus cereus* and *Streptococcus pneumonia*) and gram negative (*Escherichia coli* and *Pseudomonas aeruginosa*) bacteria, viruses, and fungi. Moreover, doped TiO_2 nanoparticles such as Ag-TiO_2 nanoparticles are exceptionally effective for inhibition multi-drug resistant bacteria growth like *Klebsiella oxytoca*, *Klebsiella pneumoniae*, *Pseudomonas aeruginosa*, *Proteus mirabilis*, *Staphylococcus aureus*, and fungal isolates including *Fusarium solani*, *Aspergillus flavus*, *Aspergillus fumigatus*, and *Aspergillus niger* [18–21].

Though TiO_2 nanoparticles have massive applicability in numerous sectors, there exist few limitations with pure TiO_2 form like inefficient visible light exploitation due to larger band gap, low adsorption capacity, and recombination of photo-generated charge carriers that influenced photocatalytic activity. To overcome these limitations, doping incorporated with metals and nonmetals has proven an effective and approachable technique that can engineer the band gap of TiO_2 nanomaterials and expands their applicability [22]. In our research, we have investigated the efficacy of photodegradation by using different dopants for band-gap engineering and making TiO_2 nanoparticles effective in VIS irradiation. We have synthesized various doped TiO_2 nanomaterials: nitrogen doped (N doped), carbon doped (C doped), iron doped (Fe doped), and silver doped (Ag doped) via the most convenient and easy "sol–gel method." This method had various advantages, such as less time to perform lowest temperature processing, composition accuracy, economic, purity, and control nanoparticle growth. The photocatalytic degradability was verified by analyzing methylene blue degradation under both UV and VIS spectral ranges. The antimicrobial properties and dye degradation potency of the differently doped nanoparticles were also verified in the paper. To verify the band-gap energy difference and other physio-chemical properties, ultraviolet–visible spectroscopy (UV–Vis), Tauc plot formation, SEM (scanning electron microscope), EDS (energy dispersive spectrophotometer), and X-ray diffraction (XRD) were performed.

2 Experimental

2.1 Materials

Titanium (IV) isopropoxide (TTIP) obtained by SRL Pvt. Ltd. was used as a titania precursor. Urea [$(NH_2)_2CO$], glucose [$C_6H_{12}O_6$], silver nitrate [$AgNO_3$], and ferrous sulphate heptahydrate [$FeSO_4.7H_2O$] from HIMEDIA were

obtained as sources of all dopants: nitrogen (N), carbon (C), silver (Ag), and iron (Fe), respectively. Methylene blue [$C_{16}H_{18}N_3S$] from SRL was used for the observation of photocatalytic activity and acid pink azo dye from Color Tax (Pvt) Ltd. for dye degradation in wastewater. Isopropyl alcohol (≧ 99.8%) was acquired for washing nanomaterials. LB (Luria Bertani) Broth, Miller from HIMEDIA, and *E. coli* (MTCC 2961) were used for the bacterial observations. All the procured chemicals were of analytical grade, and no further purification was performed. Deionized water was utilized for the preparation of all solutions and reagents throughout the process.

2.2 Methods

2.2.1 Synthesis of TiO_2 photocatalyst

Synthesis of N-, C-, Fe-, and Ag-doped TiO_2 nanoparticles was done by a simple, efficient, and modified sol–gel method. Different concentrations of all dopants were utilized for the synthesis of doped TiO_2 nanoparticles [12, 23]. About 1–4% w/v urea was dissolved in 100 mL of deionized water into a beaker and stirred for 15 min for getting N1, N2, N3, and N4, N-doped TiO_2 nanoparticles, respectively. A total of 10 mL of titanium isopropoxide (TTIP) was added dropwise to the solution to attain suspension and vigorously stirred on a magnetic stirrer (REMI 5MLH) for 30 min at 900–1000 rpm. Obtained suspensions were centrifuged at 5000 rpm for 10 min at room temperature. The supernatant was drained out, and the settled particles were washed with isopropyl alcohol and deionized water 4–5 times. The particles were dried at 40 ℃ for 15 h in a hot air oven. A similar process was applied for the preparation of C-doped, Fe-doped, and Ag-doped TiO_2 nanoparticles with addition of same percentage weight of glucose as a precursor to form C1, C2, C3, and C4, ferrous sulphate heptahydrate for Fe1, Fe2, Fe3, and Fe4 and silver nitrate for Ag1, Ag2, Ag3, and Ag4 by using silver nitrate. Undoped TiO_2 (UD) nanoparticles were procured by dissolving 10 mL of TTIP in 100 ml of deionized water, and the rest process was followed the same as doped nanoparticles.

2.2.2 Photo-absorbance and activation energy determination of the TiO_2 nanoparticles

The synthesized TiO_2 nanoparticles, both doped and undoped, were subjected to a photo-absorbance activity test. All the samples were scanned under the full wavelength range, from 200 to 1100 nm for verifying their absorbance characteristic in visible and UV ranges (ELICO Double Beam SL 210 UV–Vis spectrophotometer). The scan results were used to develop a Tauc plot to analyze the activation energy of the prepared TiO_2 samples. For the analysis of band-gap engineering of semiconductor-like material that is TiO_2, tauc plot was the appropriate method that was applicable for both types of semiconductors, that is direct and indirect [24].

2.2.3 Determination of photocatalytic activity of the TiO_2 nanoparticles

Degradation of methylene blue helped in evaluation of photocatalytic activity of all photocatalyst powders [25]. Degradation rate of methylene blue (10 mg/L) in triplicate was measured under ultraviolet (UV) light irradiation and visible light irradiation by dissolving 0.1 mg of catalyst samples (N1, N2, N3, N4, C1, C2, C3, C4, Fe1, Fe2, Fe3, Fe4, Ag1, Ag2, Ag3, Ag4) into 10 mL of methylene blue solution in test tubes. Sonication of the acquired samples was done for 1 h, 2 h, and 3 h with further shaking for 12 h at 200 rpm under a visible light source and UV light source, respectively. All samples were centrifuged at 13,000 rpm at 4 ℃ for 10 min. The optimum wavelength for methylene blue was analyzed by scanning the sample from wavelength 200 to 1100 nm. The absorption spectrums were recorded using UV–Vis spectrophotometer at 664-nm wavelength as it has shown λ-max (maximum absorption wavelength).

2.2.4 Degradation of dyes in wastewater

Dye degradation analysis was done by the removal of acid pink dye from aqueous solutions using the adsorption process based on different types of doped TiO_2 nanoparticles. This process was performed by using UV–Vis spectrophotometer with full-range scanning, from 200 to 1100 nm and at 550-nm wavelength as it shows maximum absorption wavelength (λ-max) for acid pink dye. Acid pink dye solution (0.5 g/L) was reacted by different doped TiO_2 nanoparticles with 100 mg/L concentration. All samples were kept in dark for 60 min to reach equilibrium stage, and then absorbance was noted after 60-min, 120-min, and 240-min incubation under visible light. The percentage degradation of acid pink dye was calculated by the following formula [26]:

$$\% \text{ Degradation} = \frac{\text{Initial absorbance} - \text{Final absorbance}}{\text{Initial absorbance}} * 100 \quad (1)$$

2.2.5 Determination of antimicrobial activity of TiO_2 nanoparticles

Antimicrobial activity was determined by observing MIC (minimal inhibitory concentration) in broth suspension [27]**.** Pre-inoculums were prepared by introducing 2% *E. coli* (MTCC 2961) bacterial culture into 100 ml of LB broth

medium and incubated for 24 h at 37 ℃. About 1% *E. coli* inoculums were inoculated in 10 mL of LB broth medium along with all catalyst samples separately and incubated at 37 ℃ for 150 rpm under visible light. Growth of culture was valued after incubation for a defined time period (0 h, 6 h, and 24 h).

$$\%\ \text{Inhibition} = \frac{\text{Absorbance of catalyst} - \text{Absorbance of culture (without catalyst)}}{\text{Absorbance of culture (without catalyst)}} * 100 \quad (2)$$

The percentage inhibition zone of all photocatalysts was calculated by following the above formula.

All photocatalysts were proceeded to a fine powder form for morphological analysis. In SEM/EDS analysis, an initial sample was coated with palladium by sputtering in the presence of process gas (argon gas) for 1 min. After that treated samples were scanned at optimum magnification and image was captured as per required outcomes. Simultaneous same sample was analyzed for EDS, and graphical/numerical outcomes of existing elements were observed.

3 Result and discussion

3.1 Morphological characterization

The physical and morphological characteristics of the differently doped TiO_2 nanoparticles such as structural variability, size, and crystallinity were identified with SEM–EDS analysis and XRD observation. The synthesized doped nanoparticles of carbon and iron show change in color; both the doped nanoparticles developed yellow to brown color in synthesis. The nitrogen- and silver-doped nanoparticles had retained the same white color as the undoped TiO_2 nanoparticles. The SEM analysis was performed by JSM IT500 scanning electron microscope. SEM images of the different doped nanoparticles (Fig. 1) revealed the formation of microspheres. The microsphere size length was determined for C doped as 245 µm as maximum and 79 µm minimum, with a mean of 161.72 µm. Similarly, for N doped, Ag doped, and Fe doped, the measured length was 155 as maximum and 96 µm, with a mean of 137.52 µm, 148.39 as maximum, and 96 µm, with a mean of 117.678 µm, 211 µm as maximum and 83 µm, with a mean of 102.672 µm. The EDS analysis of the doped nanoparticles confirmed the respective inclusion of dopants in the structure of TiO_2, which can be seen in Fig. 1 (e–h). Similar morphological results were reported in earlier reports [28–31].

3.1.1 XRD analysis

The crystallinity and the phase formation of the prepared TiO_2 samples were analyzed using an X-ray diffractometer (Bruker D8 advance), and further analysis was carried out by referring Habibi S. and Jamshidi M [12]. The measurements were carried out at 40 kV and 40 mA, which employed CuKα radiation at a wavelength of 0.15418 nm at an angular incidence of $2\theta = 5–80°$, with a scan step speed of 1°/min. Figure 2 represents the XRD patterns of all the synthesized doped TiO_2. The XRD diffraction pattern reveals that all the doped TiO_2 samples had retailed their crystallinity. The characteristics anatase (101) and rutile (110) could be distinctly identified for the XRD pattern in Fig. 2. The characteristic peaks at $2\theta = 25.4°$ and $2\theta = 27.5°$ for TiO_2 were observed in all the doped TiO_2 nanoparticles, thus retaining the lattice characteristics of TiO_2 particles and their photocatalytic effect. In N-doped TiO_2 nanoparticles, the anatase phase is more prominent as compared to C-, Ag-, and Fe-doped particles. The difference could be identified by the peak of $2\theta = 27.5°$, in these doped nanoparticles.

3.2 Tauc-plot for a band gap

The optical band-gap energy of undoped (UD) and doped (N1, N2, N3, N4, C1, C2, C3, C4, Fe1, Fe2, Fe3, Fe4, Ag1, Ag2, Ag3, Ag4) TiO_2 nanoparticles has been evaluated by extrapolating linear region of the plot of eV ($h\nu$) verses $(\alpha h\nu)^{1/2}$ [32]. According to previously reported literature (Aguilar et al. [33]), anatase and rutile phases of TiO_2 were considered indirect semiconductor material and followed indirect band-gap energy equations,

$$(\alpha h\nu)^n = K(h\nu - E_g) \quad (3)$$

where

"α" absorbance coefficient,

"$h\nu$" incident photon energy,

"K" energy-independent constant

"Eg" band-gap energy

"n" nature of transition ($n = 1$ for direct transition and $n = 1/2$ for indirect transition)

In tauc plot method for indirect transition, eV ($h\nu$) was plotted on x-axis and $(\alpha h\nu)^{1/2}$ on y-axis. The final equation used for tauc plot was

$$(\alpha h\nu)^{1/2} = K(h\nu - E_g) \quad (4)$$

By referring to Eq. (4) calculated, the band-gap energies were calculated for all catalysts, and the best-fit value of each

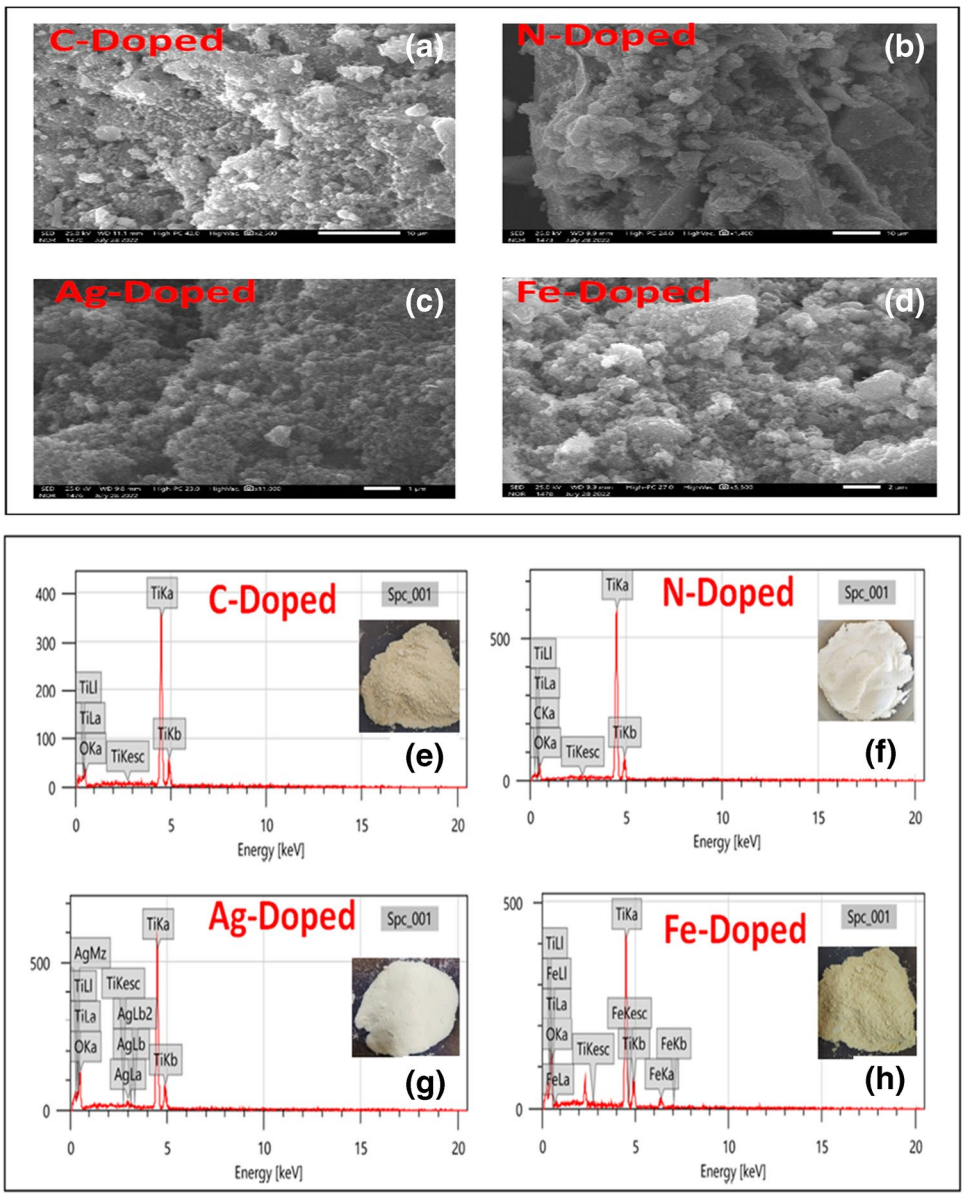

Fig. 1 SEM image of **a** C-doped TiO2, **b** N-doped TiO2, **c** Ag-doped TiO2, and **d** Fe-doped TiO2. The EDS analysis data of percentage composition of TiO2 nanoparticles with **e** doping of C, **f** doping of N, **g** doping of Ag, and **h** doping of Fe

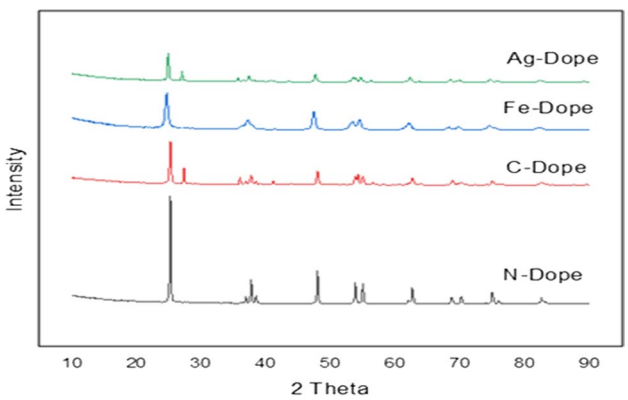

Fig. 2 XRD pattern for differently doped TiO2 nanoparticles

dopant is shown in Fig. 3. Among the N-doped TiO_2 nanoparticles, C-doped TiO_2 nanoparticles, Fe-doped TiO_2 nanoparticles, and Ag-doped TiO_2 nanoparticles with all different concentrations decreasing order of band-gap energies have been reported in the order N2 (2.1 eV) > C2 (2.8 eV) > Ag1 (2.9 eV) > Fe2 (3.0 eV). N2 nanoparticles have shown the lowest band gap among all the nanoparticles and are indicated to be the most active in the VIS range [34]. The effectivity is later verified by methylene blue degradation.

3.3 Observation of photocatalytic activity

The photocatalytic activity of C, N, Ag, Fe, and undoped TiO_2 was determined in both visible spectrum and ultraviolet spectrum for determining the dye degradability (methylene

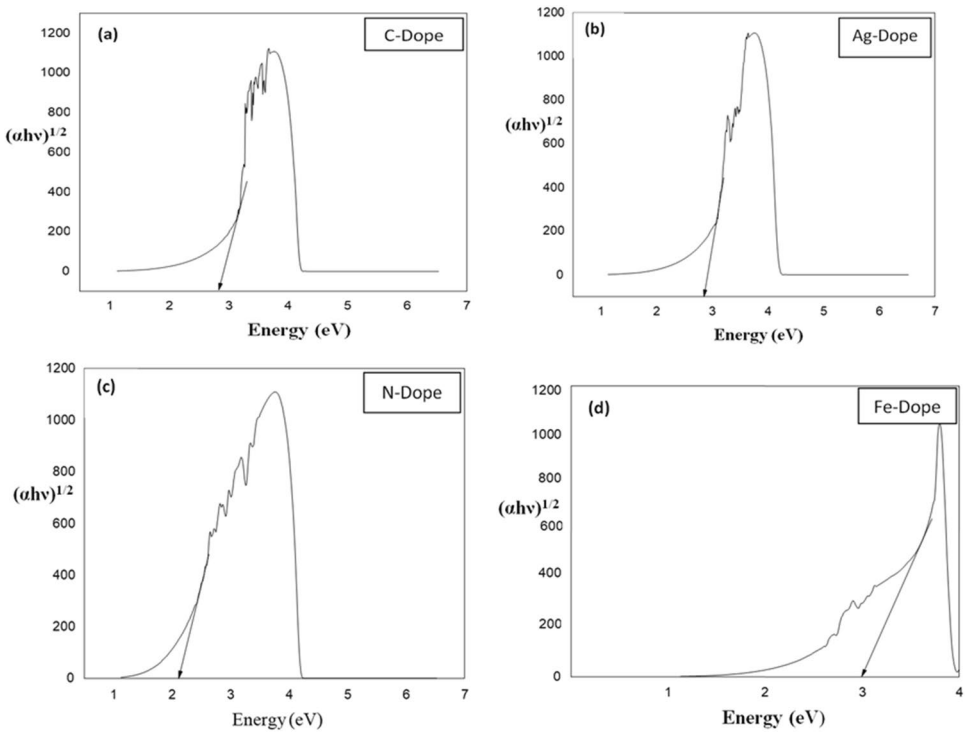

Fig. 3 Plot of eV ($h\nu$) versus ($\alpha h\nu$)1/2 to evaluate the band-gap energy of **a** C-doped TiO2 nanoparticles **b** Ag-doped TiO2 nanoparticles **c** N-doped TiO2 nanoparticles **d** Fe-doped TiO2 nanoparticles

blue) at different time exposures. The results are verified, and its efficacy was established by analysis of variance. With respect to influence of different metal and nonmetal dopants, C, N, Ag, and Fe could also improve crystallinity, increase in the specific surface area or thus, additionally, enhancing the photocatalytic performance regarding reaction time [35]. Table 1 represents the results of the degradability of methylene blue by different dopants with different dopant concentrations at respective treatment exposures at 1, 2, 3, and 12 h. From the result, it can be inferred that the exposure time for the degradation of methylene blue does not have a significant effect. The η^2 value (Table 2) of time was insignificant (value = 0.08) for the degradation, whereas the doped nanoparticles of different dopants have significant influence ($\eta^2 = 0.968$), the efficient degradation of methylene blue under visible range. Moreover, it was observed from the data that the effect of different doped nanoparticles was efficient in the photocatalytic degradation under visible range in the order N > C = Ag > Fe > undoped. So, from Table 1, it could be concluded that N-doped TiO_2 nanoparticles were more efficient in photocatalytic degradation at a visible range at any hourly treatment effect. Apart from the dopant and time factor, the analysis was also carried out for dopant percentage weight in engineered TiO_2 for organic pollutant degradation via photocatalysis at visible wavelength range. From Table 3, it could be seen that dopant percentage weights have a significant influence on the degradability of methylene blue under the visible wavelength range. It was observed that 2% and 3% N-doped TiO_2 were more significant than any other dopant or any other chosen percentage weight for the degradation. The effect of significance can be represented as 2% = 3% > 1% > 4%.

We could infer from the results of Tables 1, 2, and 3 that dopant and dopant percentage affects the photocatalytic treatment, but the treatment time is not significant after 1 h of treatment. Based on this inference, final treatment conditions were established with differently doped nanoparticles, dopant weight percentage, and exposure to visible and UV irradiation for 1 h. The results from Table 4 show under visible light irradiation N-doped TiO_2 nanoparticle of doped percentage of 2% and 3% performed best among all dopants and percentage weight. It could be concluded that N-doped TiO_2 with a dopant weight percentage of 2–3% is most efficient in methylene blue degradation. For any dye degradation, types of engineered nanoparticle ($\eta^2 = 0.997$) and percentage weight of dopant ($\eta^2 = 0.987$) are the most significant factors and the treatment in the independent time factor after the 1st hour (Table 5).

3.4 Investigating dye removal by catalysts

All developed nanoparticles show different potential toward acid pink dye. After reaching equilibrium stability, there were insignificant changes in degradation, but results received after 60 min in visible light reaction have done almost complete degradation (98.4%) of acid dye by Fe2 (iron-doped TiO_2 nanoparticles). While, among all

Table 1 Effect of different engineered nanoparticles at different time exposures under visible light irradiation

Nanoparticle	Hour	Absorbance
Ag1	1	0.243 [a]
	2	0.242 [a]
	3	0.237 [a]
	12	0.231 [a]
Ag2	1	0.283 [a]
	2	0.281 [a]
	3	0.277 [a]
	12	0.268 [a]
Ag3	1	0.299 [a]
	2	0.303 [a]
	3	0.308 [a]
	12	0.293 [a]
Ag4	1	0.309 [a]
	2	0.312 [a]
	3	0.308 [a]
	12	0.303 [a]
C1	1	0.333 [a]
	2	0.328 [a]
	3	0.328 [a]
	12	0.322 [a]
C2	1	0.232 [a]
	2	0.221 [a]
	3	0.221 [a]
	12	0.216 [a]
C3	1	0.295 [a]
	2	0.292 [a]
	3	0.293 [a]
	12	0.276 [a]
C4	1	0.314 [a]
	2	0.308 [a]
	3	0.305 [a]
	12	0.298 [a]
Fe1	1	0.477 [a]
	2	0.476 [a]
	3	0.471 [a]
	12	0.463 [a]
Fe2	1	0.474 [a]
	2	0.472 [a]
	3	0.465 [a]
	12	0.459 [a]
Fe3	1	0.493 [a]
	2	0.478 [a]
	3	0.477 [a]
	12	0.471 [a]
Fe4	1	0.493 [a]
	2	0.491 [a]
	3	0.481 [a]
	12	0.484 [a]
N1	1	0.142 [a]
	2	0.137 [a]
	3	0.136 [a]
	4	0.141 [a]
N2	1	0.132 [a]
	2	0.132 [a]
	3	0.125 [a]
	4	0.121 [a]
N3	1	0.136 [a]
	2	0.124 [a]
	3	0.123 [a]
	4	0.123 [a]
N4	1	0.146 [a]
	2	0.146 [a]
	3	0.146 [a]
	4	0.143 [a]
Blank	1	0.497 [a]
	2	0.504 [a]
	3	0.505 [a]
	4	0.504 [a]
Undoped	1	0.475 [a]
	2	0.476 [a]
	3	0.474 [a]
	4	0.475[a]
Ag		0.281[B]
C		0.286[B]
Fe		0.477[C]
N		0.135[A]
Blank		0.503[D]
Undoped		0.475[C]
	Fcal	34.715
Fcal[*]		1157.606

In a column average absorbance value followed by a common alphabet was not significantly different at $p < 0.05$

[*] Significant at $p < 0.05$

Table 2 Effect size analysis of role of different factors toward absorbance level

Factor	Fcal	η^2
Nanoparticle	1157.606[*]	0.968
Hour	0.498	0.08

η^2: partial eta square

[*] Significant at $p < 0.05$

other doped photocatalysts, N1 (1% concentration) has shown highest degradation, i.e., 87.3% in nitrogen-doped TiO_2 nanoparticles, C2 with 88.5%, and Ag2 with 87% dye degradation rate. Further reactions were performed at 120 min and 240 min with minimal changes (Fig. 4 a–d).

Table 3 Comparative analysis of effect of nanoparticle degradation with different dopant weights

Nanoparticle	Absorbance	Nanoparticle	Absorbance	Nanoparticle	Absorbance	Nanoparticle	Absorbance
N1	0.1389[b]	C1	0.3276[d]	Fe1	0.4718[a]	Ag1	0.2382[a]
N2	0.1274[a]	C2	0.2225[a]	Fe2	0.4673[a]	Ag2	0.2771[b]
N3	0.1266[a]	C3	0.2891[b]	Fe3	0.4798[b]	Ag3	0.3007[c]
N4	0.1454[c]	C4	0.3062[c]	Fe4	0.4872[c]	Ag4	0.3079[d]
Fcal*	28.4438	Fcal*	445.9296	Fcal*	14.5074	Fcal*	239.3693

In a column average absorbance value followed by a common alphabet are not significantly different at $p < 0.05$

* Significant at $p < 0.05$

Table 4 Comparative analysis of effect of nanoparticle with different dopant percentages on degradation of methylene blue at visible and UV irradiation range

Nanoparticle	Dopant wt. (%)	Visible range	UV range
Ag	1	0.231 [a]	0.189 [a]
	2	0.293 [b]	0.252 [b]
	3	0.306 [b]	0.293 [c]
	4	0.301 [b]	0.299 [c]
C	1	0.318 [b]	0.289 [b]
	2	0.218 [a]	0.23 [a]
	3	0.213 [a]	0.347 [c]
	4	0.313 [b]	0.389 [d]
Fe	1	0.478 [b]	0.323 [c]
	2	0.466 [a]	0.301 [a]
	3	0.458 [a]	0.311 [b]
	4	0.479 [b]	0.364 [d]
N	1	0.145 [b]	0.167 [c]
	2	0.129 [a]	0.15 [a]
	3	0.136 [a]	0.161 [b]
	4	0.148 [b]	0.196 [d]
Ag		0.283 [C]	0.258 [B]
C		0.265 [B]	0.314 [C]
Fe		0.47 [D]	0.325 [D]
N		0.139 [A]	0.168 [A]
	Fcal	79.763	812.177
Fcal*		6019.66	3199.625

In a column average absorbance value followed by a common alphabet was not significantly different at $p < 0.05$

* Significant at $p < 0.05$

Table 5 Effect size analysis of role of different factors toward absorbance level

	Visible range		UV range	
Factor	Fcal	η^2	Fcal	η^2
Dopant wt	79.763	0.882	812.177*	0.987
Nanoparticle	6019.66	0.998	3199.625*	0.997

η^2: partial eta square

* Significant at $p < 0.05$

3.5 Antimicrobial activity

Synthesized samples supported the antibacterial activity under the visible light because of improved photocatalytic activity and observed by minimal inhibitory concentration [36]. By Swain et al. [37], initial and final concentrations of all samples were analyzed before the reactions started by UV–Vis spectrophotometer at 600-nm wavelength (Fig. 5). Growth analyses of samples were recorded after 6 h and 24 h. After 6-h incubation, all Ag-doped TiO_2 nanoparticles showed almost complete inhibitory after this Fe2 registered the lowest minimal inhibitory concentration of 37.95% (possible killing mechanisms of bacteria) calculated by Eq. (b). Similarly, for the 24-h incubation, Ag-doped TiO_2 nanoparticles completely inhibit the growth of bacterial strain because Ag NPs itself shows great antimicrobial and drug delivery potential, with the mechanism that silver nanoparticles were associated with the production of free radicals and proceeding free-radical-induced oxidative damage of the cell membranes of bacteria, and N2 showed the lowest minimal inhibitory concentration of 29.2% (possible killing mechanisms of bacteria) [38–40].

This work has shown that major drawback of TiO_2 (i.e., higher band gap) has been overcome by applying a very simple and effective doping method. Now, these modified doped TiO_2 nanoparticles have vast relevancy and potential to reach out a broad domain of applications. They can be successfully utilized for soil remediation, phenol degradation, CO_2 reduction, Cr(VI) reduction, H_2 production, wastewater treatment, air purification, and many more. Moreover, TiO_2 is a very convincible photocatalyst that can be customized and modified according to targeted issues [41, 42].

4 Conclusion

Corroboration of all results represented that N2 has shown to be the best and lowest band gap, i.e., 2.1 eV and also confirmed for 74% degradation rate of methylene blue. A

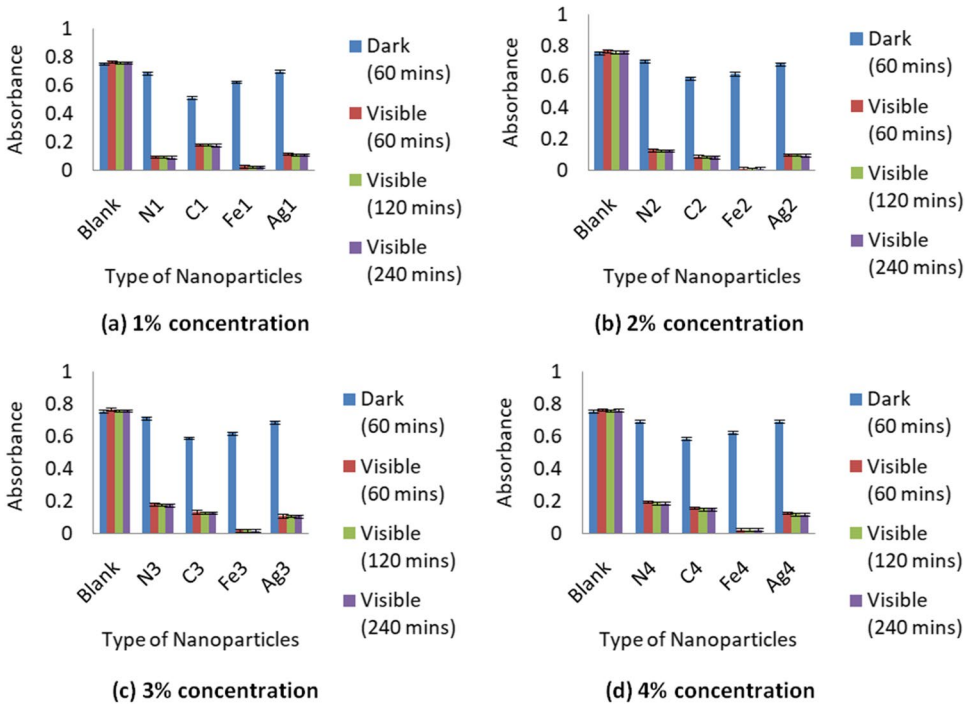

Fig. 4 Dye degradation by all photocatalysts at different time intervals under visible light (**a**–**d**)

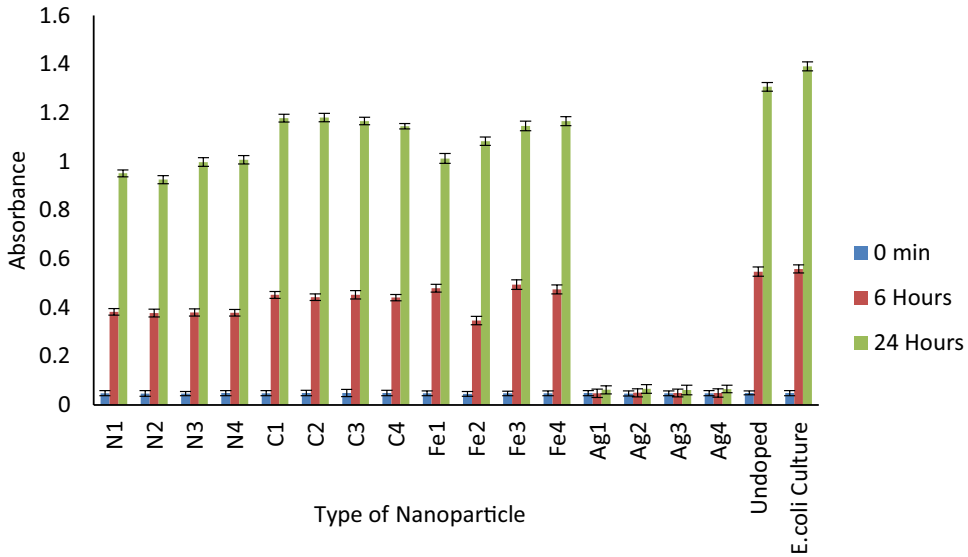

Fig. 5 Minimal inhibitory concentration of all photocatalysts at different time intervals under visible light

total of 98.4% degradation industrial acid pink azo dye was registered by Fe2 photocatalytic. In aspect of antimicrobial activities, Ag-TiO_2 has shown complete inhibition, followed by N2 with 70.8% inhibition. Relatively, all observations suggested that type and amount of dopant influenced the activity of photocatalysts. The study may be extended for wide applications in natural light (as UV spectrum is not a barrier) right from surface reaction to pollutant abetment in air and expanded to industrial application via a product form.

Acknowledgements The authors are indebted to the Department of Science and Technology (DST), Govt. of India New Delhi, for providing financial support to the project SP/YO/543/2018, focusing on the development of low-cost domestic filters for arsenic remediation. Aakanksha Rajput and Arindam Kuila are thankful to Vice Chancellor of Banasthali Vidyapith for necessary infrastructure and facilities to complete this work.

Author contribution Aakanksha Rajput and Md Hafizur Rahman performed all the experiments. Md Azizur Rahman and Arindam Kuila planned the work and wrote the manuscript.

Data availability This submitted article contains all of the data generated or analyzed during this investigation.

Declarations

Ethical approvals Not applicable.

Conflict of interest The authors declare no competing interests.

References

1. Krishnan S, Shriwastav A (2021) Application of TiO2 nanoparticles sensitized with natural chlorophyll pigments as catalyst for visible light photocatalytic degradation of methylene blue. J Environ Chem Eng 9(1):104699. https://doi.org/10.1016/j.jece.2020.104699
2. Dubey RS, Krishnamurthy KV, Singh S (2019) Experimental studies of TiO2 nanoparticles synthesized by sol-gel and solvothermal routes for DSSCs application. Results Phys 14:102390. https://doi.org/10.1016/j.rinp.2019.102390
3. Khan MM, Ansari SA, Pradhan D, Ansari MO, Lee J, Cho MH (2014) Band gap engineered TiO2 nanoparticles for visible light induced photoelectrochemical and photocatalytic studies. J Mater Chem A 2(3):637–644. https://doi.org/10.1039/C3TA14052K
4. Allen NS, Mahdjoub N, Vishnyakov V, Kelly PJ, Kriek RJ (2018) The effect of crystalline phase (anatase, brookite, and rutile) and size on the photocatalytic activity of calcined polymorphic titanium dioxide (TiO2). Polym Degrad Stab 150:31–36. https://doi.org/10.1016/j.polymdegradstab.2018.02.008
5. Rueda D, Arias V, Zhang Y, Cabot A, Agudelo AC, Cadavid D (2020) Low-cost tangerine peel waste mediated production of titanium dioxide nanocrystals: synthesis and characterization. Environ Nanotechnol Monit Manag 13:100285. https://doi.org/10.1016/j.enmm.2020.100285
6. Singh R, Dutta S (2018) Synthesis and characterization of solar photoactive TiO2 nanoparticles with enhanced structural and optical properties. Adv Powder Technol 29(2):211–219. https://doi.org/10.1016/j.apt.2017.11.005
7. Abbad S, Guergouri K, Gazaout S, Djebabra S, Zertal A, Barille R, Zaabat M (2020) Effect of silver doping on the photocatalytic activity of TiO2 nanopowders synthesized by the sol-gel route. J Environ Chem Eng 8(3):103718. https://doi.org/10.1016/j.jece.2020.103718
8. Daram P, Banjongprasert C, Thongsuwan W, Jiansirisomboon S (2016) Microstructure and photocatalytic activities of thermal sprayed titanium dioxide/carbon nanotubes composite coatings. Surf Coat Technol 306:290–294. https://doi.org/10.1016/j.surfcoat.2016.06.068
9. Lettieri S, Gargiulo V, Alfè M, Amati M, Zeller P, Maraloiu VA, ... Maddalena P (2020) Simple ethanol refluxing method for production of blue-colored titanium dioxide with oxygen vacancies and visible light-driven photocatalytic properties. J Phys Chem C 124(6): 3564-3576. https://doi.org/10.1021/acs.jpcc.9b08993
10. Nachit W, Ahsaine HA, Ramzi Z, Touhtouh S, Goncharova I, Benkhouja K (2022) Photocatalytic activity of anatase-brookite TiO2 nanoparticles synthesized by sol gel method at low temperature. Opt Mater 129:112256. https://doi.org/10.1016/j.optmat.2022.112256
11. Zhao Y, Li Y, Wang C.W, Wang J, Wang XQ, Pan Z.W, ... Zhou F (2013) Carbon-doped anatase TiO2 nanotube array/glass and its enhanced photocatalytic activity under solar light. Solid State Sci 15: 53–59. https://doi.org/10.1016/j.solidstatesciences.2012.08.008
12. Habibi S, Jamshidi M (2019) Sol–gel synthesis of carbon-doped TiO2 nanoparticles based on microcrystalline cellulose for efficient photocatalytic degradation of methylene blue under visible light. Environ Technol. https://doi.org/10.1080/09593330.2019.1604815
13. Sood S, Umar A, Mehta SK, Kansal SK (2015) Highly effective Fe-doped TiO2 nanoparticles photocatalysts for visible-light driven photocatalytic degradation of toxic organic compounds. J Colloid Interface Sci 450:213–223. https://doi.org/10.1016/j.jcis.2015.03.018
14. Marques J, Gomes TD, Forte MA, Silva RF, Tavares CJ (2019) A new route for the synthesis of highly-active N-doped TiO2 nanoparticles for visible light photocatalysis using urea as nitrogen precursor. Catal Today 326:36–45. https://doi.org/10.1016/j.cattod.2018.09.002
15. Mehra S, Singh M, Chadha P (2021) Adverse impact of textile dyes on the aquatic environment as well as on human beings. Toxicol Int 28(2):165–176. https://doi.org/10.18311/ti/2021/v28i2/26798
16. Ancy K, Bindhu MR, Bai JS, Gatasheh MK, Hatamleh AA, Ilavenil S (2022) Photocatalytic degradation of organic synthetic dyes and textile dyeing waste water by Al and F co-doped TiO2 nanoparticles. Environ Res 206:112492. https://doi.org/10.1016/j.envres.2021.112492
17. Mohammed AK, Salh KK, Ali FA (2021) ZnO, TiO2 and Ag nanoparticles impact against some species of pathogenic bacteria and yeast. Cell Mol Biol 67(3):24–34. https://doi.org/10.14715/cmb/2021.67.3.4
18. Ananpattarachai J, Boonto Y, Kajitvichyanukul P (2016) Visible light photocatalytic antibacterial activity of Ni-doped and N-doped TiO2 on Staphylococcus aureus and Escherichia coli bacteria. Environ Sci Pollut Res 23(5):4111–4119. https://doi.org/10.1007/s11356-015-4775-1
19. Ancy K, Vijilvani C, Bindhu MR, Bai SJS, Almaary KS, Dawoud TM ... Alfadul MS (2021) Visible light assisted photocatalytic degradation of commercial dyes and waste water by Sn–F co-doped titanium dioxide nanoparticles with potential antimicrobial application. Chemosphere 277:130247. https://doi.org/10.1016/j.chemosphere.2021.130247
20. Rangayasami A, Kannan K, Subban M (2021) December) Bio-engineered TiO2 nanoparticles using Andrographis alata (Vahl) Nees leaf extract and their antibacterial and anticancer activities. In Macromolecular Symposia 400(1):2100085. https://doi.org/10.1002/masy.202100085
21. Aguda ON, Lateef A (2022) Valorization of Parkia biglobosa wastewater for novel biofabrication of Ag/TiO2 nanoparticles with potent action against MDR strains and nanotextile application. Inorg Chem Commun 140:109427. https://doi.org/10.1016/j.inoche.2022.109427
22. Peiris S, de Silva HB, Ranasinghe KN, Bandara SV, Perera IR (2021) Recent development and future prospects of TiO2 photocatalysis. J Chin Chem Soc 68(5):738–769. https://doi.org/10.1002/jccs.202000465
23. Negi C, Kandwal P, Rawat J, Sharma M, Sharma H, Dalapati G, Dwivedi C (2021) Carbon-doped titanium dioxide nanoparticles for visible light driven photocatalytic activity. Appl Surf Sci 554:149553. https://doi.org/10.1016/j.apsusc.2021.149553
24. Phan TD, Vo CM, Tran TMT, Luu TLA, Nguyen XS (2019) Structural and bandgap properties of titanium dioxide nanotube/graphene oxide composites prepared by a facile hydrothermal method. Mater Res Express 6(10):105054. https://doi.org/10.1088/2053-1591/ab3a0b
25. Jeon JP, Kweon DH, Jang BJ, Ju MJ, Baek JB (2020) Enhancing the photocatalytic activity of TiO2 catalysts. Adv Sustain Syst 4(12):2000197. https://doi.org/10.1002/adsu.202000197

26. Ahmadi S, Mohammadi L, Rahdar A, Rahdar S, Dehghani R, Adaobi Igwegbe C, Kyzas GZ (2020) Acid dye removal from aqueous solution by using neodymium (III) oxide nanoadsorbents. Nanomaterials 10(3):556. https://doi.org/10.3390/nano10030556
27. Vassallo J, Besinis A, Boden R, Handy RD (2018) The minimum inhibitory concentration (MIC) assay with Escherichia coli: an early tier in the environmental hazard assessment of nanomaterials. Ecotoxicol Environ Saf 162:633–646. https://doi.org/10.1016/j.ecoenv.2018.06.085
28. Singh S, Perween S, Ranjan A (2021) Enhancing the visible light induced photocatalytic activity in sol-electrospun zinc titanate nanopowders by nitrogen doping. J Phys Chem Solids 158:110221. https://doi.org/10.1016/j.jpcs.2021.110221
29. Kamaludin R, Othman MHD, Kadir SHSA, Ismail AF, Rahman MA, Jaafar J (2018) Visible-light-driven photocatalytic N-doped TiO2 for degradation of bisphenol A (BPA) and reactive Black 5 (RB5) dye. Water Air Soil Pollut 229(11):1–11. https://doi.org/10.1007/s11270-018-4006-8
30. Mohamed MA, Salleh WNW, Jaafar J, Ismail AF, Abd Mutalib M, Jamil SM (2015) Incorporation of N-doped TiO2 nanorods in regenerated cellulose thin films fabricated from recycled newspaper as a green portable photocatalyst. Carbohyd Polym 133:429–437. https://doi.org/10.1016/j.carbpol.2015.07.057
31. Ruan P, Qian J, Xu Y, Xie H, Shao C, Zhou X (2013) Mixed-phase TiO2 nanorods assembled microsphere: crystal phase control and photovoltaic application. CrystEngComm 15(25):5093–5099. https://doi.org/10.1039/C3CE40351C
32. Murphy AB (2007) Band-gap determination from diffuse reflectance measurements of semiconductor films, and application to photoelectrochemical water-splitting. Sol Energy Mater Sol Cells 91(14):1326–1337. https://doi.org/10.1016/j.solmat.2007.05.005
33. Aguilar T, Navas J, Alcántara R, Fernández-Lorenzo C, Gallardo JJ, Blanco G, Martín-Calleja J (2013) A route for the synthesis of Cu-doped TiO2 nanoparticles with a very low band gap. Chem Phys Lett 571:49–53. https://doi.org/10.1016/j.cplett.2013.04.007
34. Pelaez M, Falaras P, Likodimos V, Kontos AG, Armah A, O'shea K, Dionysiou DD (2010) Synthesis, structural characterization and evaluation of sol–gel-based NF-TiO2 films with visible light-photoactivation for the removal of microcystin-LR. Appl Catal B 99(3–4):378–387. https://doi.org/10.1016/j.apcatb.2010.06.017
35. Piątkowska A, Janus M, Szymański K, Mozia S (2021) C-, N-, and S-doped TiO2 photocatalysts: a review. Catalysts 11(1):144. https://doi.org/10.3390/catal11010144
36. Anbumani D, vizhi Dhandapani K, Manoharan J, Babujanarthanam R, Bashir AKH, Muthusamy K... Kanimozhi K (2022) Green synthesis and antimicrobial efficacy of titanium dioxide nanoparticles using Luffa acutangula leaf extract. J King Saud Univ Sci 34(3): 101896. https://doi.org/10.1016/j.jksus.2022.101896
37. Swain P, Nayak SK, Sasmal A, Behera T, Barik SK, Swain SK ... Jayasankar P (2014) Antimicrobial activity of metal based nanoparticles against microbes associated with diseases in aquaculture. World J Microbiol Biotechnol 30(9): 2491–2502. https://doi.org/10.1007/s11274-014-1674-4
38. Ali T, Ahmed A, Alam U, Uddin I, Tripathi P, Muneer M (2018) Enhanced photocatalytic and antibacterial activities of Ag-doped TiO2 nanoparticles under visible light. Mater Chem Phys 212:325–335. https://doi.org/10.1016/j.matchemphys.2018.03.052
39. Ahmad MA, Yuesuo Y, Ao Q, Adeel M, Hui ZY, Javed R (2019) Appraisal of comparative therapeutic potential of undoped and nitrogen-doped titanium dioxide nanoparticles. Molecules 24(21):3916. https://doi.org/10.3390/molecules24213916
40. Mohammad MR, Ahmed DS, Mohammed MK (2019) Synthesis of Ag-doped TiO2 nanoparticles coated with carbon nanotubes by the sol–gel method and their antibacterial activities. J Sol-Gel Sci Technol 90(3):498–509. https://doi.org/10.1007/s10971-019-04973-w
41. Ijaz M, Zafar M (2021) Titanium dioxide nanostructures as efficient photocatalyst: progress, challenges and perspective. Int J Energy Res 45(3):3569–3589. https://doi.org/10.1002/er.6079
42. Li R, Li T, Zhou Q (2020) Impact of titanium dioxide (TiO2) modification on its application to pollution treatment-a review. Catalysts 10(7):804. https://doi.org/10.3390/catal10070804